JVSTA
JOURNAL OF VACUUM SCIENCE AND TECHNOLOGY A

Measurements of time varying plasma potential, temperature, and density in a 13.56 MHz radiofrequency discharge

Jeffrey L. Wilson, J. B. O. Caughman, Phi Long Nguyen, and D. N. Ruzic

Citation: J. Vac. Sci. Technol. A **7**, 972 (1989); doi: 10.1116/1.575830
View online: http://dx.doi.org/10.1116/1.575830
View Table of Contents: http://avspublications.org/resource/1/JVTAD6/v7/i3
Published by the AVS: Science & Technology of Materials, Interfaces, and Processing

---

Related Articles

Can surface cracks and unipolar arcs explain breakdown and gradient limits?
J. Vac. Sci. Technol. A 31, 011302 (2013)

Mechanically robust silica-like coatings deposited by microwave plasmas for barrier applications
J. Vac. Sci. Technol. A 30, 061502 (2012)

Spatially resolved measurements of ion density and electron temperature in a dual-frequency capacitively coupled plasma by complete floating double probe technique
J. Vac. Sci. Technol. A 29, 011006 (2011)

High etching rates of bulk Nb in Ar/Cl2 microwave discharge
J. Vac. Sci. Technol. A 27, 301 (2009)

Study of fluorocarbon plasma in 60 and 100MHz capacitively coupled discharges using mass spectrometry
J. Vac. Sci. Technol. A 26, 1198 (2008)

Additional information on J. Vac. Sci. Technol. A

Journal Homepage: http://avspublications.org/jvsta
Journal Information: http://avspublications.org/jvsta/about/about_the_journal
Top downloads: http://avspublications.org/jvsta/top_20_most_downloaded
Information for Authors: http://avspublications.org/jvsta/authors/information_for_contributors

ADVERTISEMENT

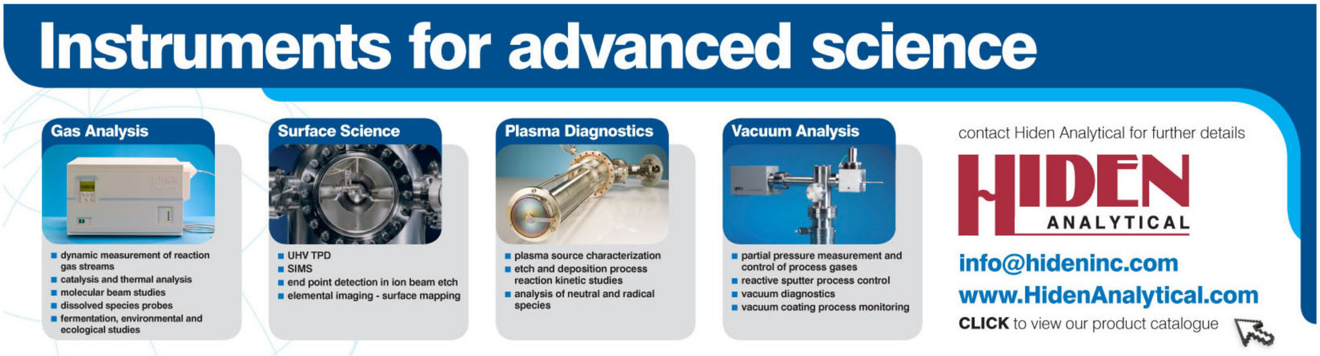

Instruments for advanced science

Gas Analysis
- dynamic measurement of reaction gas streams
- catalysis and thermal analysis
- molecular beam studies
- dissolved species probes
- fermentation, environmental and ecological studies

Surface Science
- UHV TPD
- SIMS
- end point detection in ion beam etch
- elemental imaging - surface mapping

Plasma Diagnostics
- plasma source characterization
- etch and deposition process reaction kinetic studies
- analysis of neutral and radical species

Vacuum Analysis
- partial pressure measurement and control of process gases
- reactive sputter process control
- vacuum diagnostics
- vacuum coating process monitoring

contact Hiden Analytical for further details
HIDEN ANALYTICAL
info@hideninc.com
www.HidenAnalytical.com
CLICK to view our product catalogue

Downloaded 24 Dec 2012 to 192.17.144.119. Redistribution subject to AVS license or copyright; see http://avspublications.org/jvsta/about/rights_and_permissions

Measurements of time varying plasma potential, temperature, and density in a 13.56 MHz radio-frequency discharge

Jeffrey L. Wilson, J. B. O. Caughman II, Phi Long Nguyen, and D. N. Ruzic
Nuclear Engineering Department, University of Illinois, Urbana, Illinois 61801

(Received 13 December 1988; accepted 16 January 1989)

Argon plasma measurements were conducted in a commercial capacitively coupled etcher operating at 400 mTorr with 60-W coupled power at 13.56 MHz. Time varying floating potential was measured using a capacitively coupled probe which uses a capacitive voltage divider and a field effect transistor buffer amplifier. Average floating potential was obtained from a high-input-impedance Langmuir probe. The floating potential was found to be sinusoidal, $[21 \sin(\omega t) - 4]\,V \pm 1.5$ V, with a maximum of 17 ± 1.5 V and a minimum of -25 ± 1.5 V. From these data and the use of a low-input-impedance Langmuir probe, a calibrated instantaneous I–V characteristic is used to obtain plasma potential and electron temperature. Plasma potential was found to be sinusoidal, $[21 \sin(\omega t) + 30]\,V \pm 1.6$ V, with a maximum of 51 ± 1.6 V and a minimum of 9 ± 1.6 V. Electron temperatures were 6.58 ± 0.19 eV at maximum plasma potential and 6.49 ± 0.19 eV at minimum plasma potential. The electron density for this experiment was determined to be $1.48 \pm 0.83 \times 10^{10}$ electrons/cm^3.

I. INTRODUCTION

In this research the time varying plasma potential, electron temperature, and density in a rf discharge device were determined. These quantities are essential to the understanding of the process plasma. Accurate indication of temperature can lead to a better understanding of electron energy distribution and impact ionization reaction rate constants. Accurate indication of the plasma potential can lead to a better characterization of ion energies incident on the electrodes or substrates.

The current versus voltage (I–V) characteristics of a Langmuir probe have proven to be a useful and practical plasma diagnostic technique.[1-8] Popular Langmuir probe techniques include measuring I-V characteristics on a time scale which is short in comparison with the rf period,[5-7] time averaged I-V characteristics,[9] and double-probe methods.[5,7,10,11] Another novel idea involves using a single Langmuir probe that simultaneously measures instantaneous current and floating potential to obtain a single instantaneous I–V characteristic.[12] Effects of rf on the characteristic of a Langmuir probe has been considered by others.[5,9,11-14] Other methods for measuring plasma potential in rf plasmas include the use of high-impedance capacitive voltage divider probes,[15,16] and emissive probes.[17-21] A recent comparison of measurements of plasma potential using collecting and emitting probes has been conducted.[22] Also a comparison of various Langmuir probe techniques has recently been addressed by Chen.[12] Our method of measurement involves a combination of a two shielded Langmuir probes and a capacitive probe.

II. THEORY

General probe theory[4] uses a number of assumptions: the plasma is a homogeneous and quasineutral composition of electrons, and singly charged positive ions of the background gas; the electrons and ions possess Maxwellian velocity distributions with characteristic temperatures T_e and T_i, respectively, with $T_e \gg T_i$; the interaction mean free paths are large compared with both the probe dimension R_p and the plasma Debye shielding length l_d (i.e., low-pressure, collisionless sheath approximation); electrons and ions which hit the probe surface are absorbed; well-defined space-charge sheaths surround the probe surface; and the probe does not perturb the plasma.

In order to more accurately reflect plasma behavior in this experiment, some of these assumptions need to be examined. To truly define an electron temperature a Maxwellian distribution must be assumed. But the electron energy distribution may deviate measurably from a Maxwellian. Therefore the electron temperatures obtained here are merely some measure of the mean electron energy. Another assumption is the "well-defined thin sheath formation." In general, the size of the sheath is voltage dependent, and especially for ion collection the sheath cannot be regarded as "thin." Hence the Bohm sheath criterion is incorporated to account for presheath effects[12] and to provide a better estimate of ion saturation.

For the gas pressure used, 400 mTorr, the mean free path for interaction, ~0.39 mm, is on the order of the probe characteristic dimension of 0.19 mm. Therefore to correct for moderate collisional effects in intermediate pressure discharges when determining the electron density from ion saturation, a scaling parameter based on the ratio R_p/l_d should be used.[24] When ion collection is not orbital motion limited, but is affected by presheath acceleration and assuming a collisionless sheath, a modified expression for ion saturation current can be obtained:

$$I_{i\,\mathrm{sat}} = (eN_eA_p/4)\,\mathrm{sqrt}[\,(8kT_e)/(\pi M_i)\,]\,j_i^*\,,$$

where j_i^* is a dimensionless ion current scale factor.

The dimensionless scale factor j_i^*, takes into account the changing size of the ion sheath/presheath as probe voltage with respect to the reference electrode changes. The Laframboise results[25] were employed, where, for large values of

$R_p/l_d, j_i^*$ represents the near sheath limited form of ion collection. When R_p/l_d is zero, j_i^* represents the orbital motion limited form of ion collection at the probe. The Laframboise technique is a numerical analysis based upon a Maxwellian electron energy distribution and assumes a collisionless sheath. Notice also that Eq. (1) incorporates the Bohm criterion.

Figure 1 shows a typical I–V characteristic curve for a dc discharge. When a probe is connected to a measuring resistor, the operating point of the circuit is given by the intersection of a load line with the I–V characteristic.[12,23] The load lines in Fig. 1(a) have negative slope since electron current is defined as positive. For accurate current measurements the load resistor R must be very small to establish a vertical load line. For accurate V_f measurements R must be very large to establish a horizontal load line. The actual current I_A and measured current I'_A are shown in Fig. 1. Similarly, the actual floating potential V_f versus measured V'_f is also shown in Fig. 1.

For rf plasmas, the I–V characteristic is sensitive to plasma sheath impedance and the probe circuits impedance to ground.[12] The load line is a function of the probe circuits input impedance. For current measurements, R should be much less than the characteristic impedance of the plasma sheath during the ion saturation region, and for V_f measurements, R should be much larger than the characteristic impedance of the plasma sheath at V_f.[12] However, when high-frequency rf is present, stray capacitance to ground normally results in an ac impedance to ground which can be much smaller than the circuit input impedance. Therefore, when measuring fluctuations in V_f, the frequency response of the circuit is limited.[12] To overcome this problem a capacitive probe was used to measure time varying V_f, rather than the standard capacitive neutralization technique.[12,26] A high-input-impedance Langmuir probe was then used to obtain a dc reference to V_f, since the V_f dc offset is not time-response limited by stray cable capacitance.

For 13.56-MHz discharges, plasma potential V_p is generally thought to vary sinusoidally with some amplitude $V_{\rm rf}$.[8] Instantaneous current will fluctuate because V_p is fluctuating. Thus the probe I–V characteristic will shift back and forth along the V axis[7] as shown in Fig. 2(a). The left-hand portion of this figure is the instantaneous I–V characteristic when the plasma is at its minimum plasma potential $(V_p)_{\rm min}$, and the right-hand portion is instantaneous I–V at maximum plasma potential $(V_p)_{\rm max}$. The actual I–V characteristic sweeps back and forth between the two indicated extremes. The average I-V of the two extremes is also shown in Fig. 2(a). Since the I–V characteristic is nonlinear, the average current will not be the same as the instantaneous current at any given voltage V. Therefore, basing calculations on average probe current could lead to an erroneous indication of plasma parameters in some cases.

The instantaneous I–V curve shown in Fig. 2(a) is derived from the instantaneous scope current trace shown on Fig. 2(b). Points I_A and I_B correspond to instantaneous current at minimum and maximum plasma potential for a specified probe bias. As probe bias is varied the instantaneous I–V curve is mapped out.

III. EXPERIMENTAL

Figure 3 shows the experimental arrangement used for this paper. A major component is the Davis and Wilder model 425 parallel-plate plasma etcher. This system consists of cylindrical process chamber, roughing pump, blower, motorized flow control valve, and water-cooled parallel plates that were ~70.1 cm in diameter and spaced 4 cm apart. The top plate was the powered electrode and the bottom the grounded electrode, which was electrically connected to the chamber chassis. A glass plate lies above the top electrode and radially along the inside cylindrical wall. Probe access was through three radial ports located approximately midplane between the two electrodes. Pressure was maintained within the chamber at 400 ± 5 mTorr as indicated by a Baratron gauge.

A Tegal 300-W 13.56-MHz generator supplied power through an associated Tegal matching network. The 13.56-MHz signal was generated within a 120-Hz sawtooth ramp. This was a peculiar characteristic of the power supply and care was taken to perform all measurements at the same

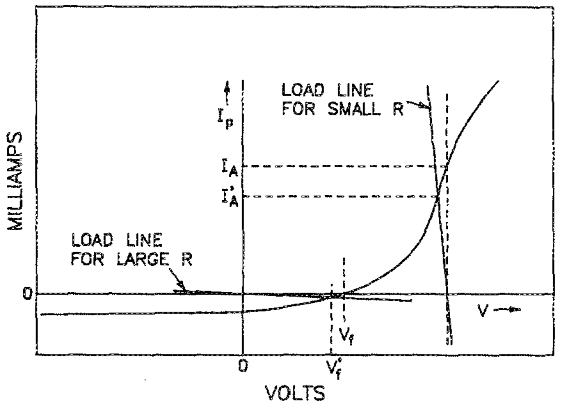

FIG. 1. Typical Langmuir probe I–V trace showing load lines. A load line with small R indicates instantaneous current. A load line with large R indicates V_f. The departure from the actual current I_A vs measured current I'_A; and actual V_f vs measured V'_f is shown.

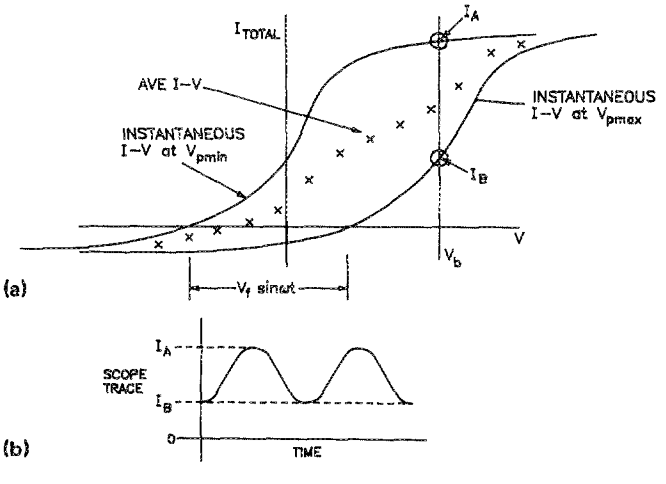

FIG. 2. (a) Instantaneous and average current vs voltage showing a vertical load line at V_b. (b) Typical scope trace of instantaneous current. I_A occurs at $(V_p)_{\rm min}$ and I_B occurs at $(V_p)_{\rm max}$ for an applied bias voltage V_b.

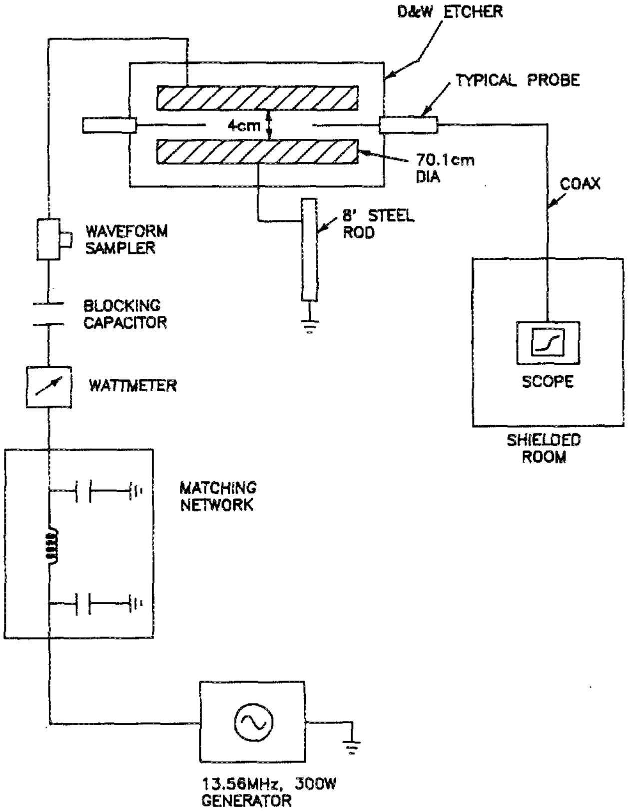

FIG. 3. Experimental arrangement. All grounds are single point connected to the steel rod.

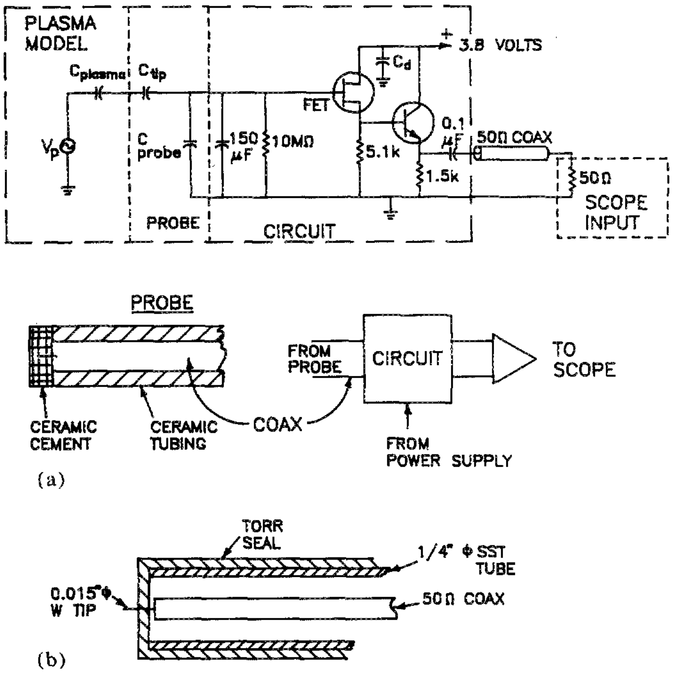

FIG. 4. Capacitive probe circuit showing the plasma as a rf source with sheath capacitance: (a) capacitive probe construction and (b) Langmuir probe construction.

point during this ramp cycle. Power was monitored by a Bird rf directional Thruline wattmeter, model 4342. The voltage waveform at the powered electrode was monitored through a capacitively coupled Bird waveform sampler and measured on a Tektronics model 475 oscilloscope. A blocking capacitor was located between the waveform sampler and the powered electrode. The dc offset bias between the powered electrode and ground was measured by a digital Fluke multimeter. Measurements of plasma parameters were taken within a double-shielded copper-screen room (Faraday cage). The power supply, rf matching network, grounded electrode, etcher chamber, cable shielding, screen room, and measurements were all referenced to a single-point ground system, which was a single 8-ft steel rod driven into the ground near the etching chamber. The grounding system greatly reduced the measurement signal noise interference associated with rf radiation. The power from the wall outlets into the screen room was passed through a low-pass filter.

Three types of probe arrangements were used to obtain plasma parameter data. A capacitive probe measured time varying floating potential, a high-input-impedance Langmuir probe obtained a reference to the time varying floating potential, and a low-input-impedance Langmuir probe measured instantaneous time varying current.

Figure 4(a) shows the capacitive probe construction and circuit schematic. This probe, when inserted within the plasma, behaves like a coaxial capacitor that tracks variations in V_f without significantly loading the plasma.[15] The probe consisted of a coaxial cable within a ceramic tubing having its extended center conductor capped with ceramic cement. A capacitive voltage divider network is formed by the probes tip capacitance and circuit capacitance from which the input signal is fed through a high input impedance field effect transistor (FET) buffer, and a NPN-transistor amplifier and delivered to a 50-Ω load. The effect of stray capacitance is minimized by locating the probe circuitry close to the probe tip. The measurement of time varying plasma potential is taken within a shielded room. This probe, its circuitry, associated power supply, and cabling were calibrated at 13.56 MHz.

The Langmuir probe construction is shown in Fig. 4(b). This probe consisted of a coaxial cable running the full length of the probe and terminated with a 15-mil tungsten tip. The coaxial cable is sleeved within a ceramic coated stainless-steel tube which is welded to a $\frac{3}{4}$-in.-o.d. tube to match the probe port. The low input impedance probe had a 50-Ω load and the high input impedance used a 1M-Ω load. The bias for the low input impedance probe varied from -50 to $+56$ V. The probe, power supply, and cabling were calibrated at 13.56 MHz.

IV. RESULTS

An argon rf discharge was maintained at 400 ± 5 mTorr. Power to the plasma discharge was maintained at 100 W forward and 40 W reverse. The voltage to the powered electrode was 72 ± 1 V p–p with a dc offset of -2 ± 0.5 V. From the calibrated capacitive probe measurement a time varying floating potential of 42.1 ± 1.6 V was obtained. Its waveform was sinusoidal and not affected by variations in bias potential. The dc reference was determined to be -4 ± 0.7 V dc. In general $V_f = [21.05 \sin(wt) - 4] V \pm 1.5$ V.

Plasma potential was graphically determined from the

I–V characteristic curve at a bias of 34 ± 0.5 V. By adding this voltage to the floating potential variation, the plasma potential was found to vary from a maximum of 51 ± 1.6 V to a minimum of 9 ± 1.6 V. In general the plasma potential can be characterized as $[21.05\sin(\omega t)+30]V\pm 1.6$ V. These measurements correspond to plasma potential variation at the midplane region between the two parallel plates. Figure 5 shows these results on a plot of a theoretical cross-sectional plasma variation between two parallel plates.

The *I–V* curve was obtained from the low-input-impedance Langmuir probe. Depending upon the bias potential applied, a sinusoidal or sinusoidal-like waveform was traced on the oscilloscope. These results are shown in Fig. 6(a) without modification for time varying floating potential. Each curve corresponds to instantaneous total probe collection current as bias potential was varied from − 50 to + 56 V dc. The upper curve corresponds to plasma conditions at minimum plasma potential and the lower to maximum plasma potential.

From this plot it appears that plasma potential is reached when the bias is at 34 V, since at this point there is clear indication of a discontinuity from an exponential region to a diverging linearlike region. Also note, since these data are uncalibrated with respect to measured floating potential, the left hand curve never goes below 0. By definition at V_f electron current and ion current are equal, i.e., total probe current is zero. Therefore an independent measurement of V_f (the capacitive probe) is used to reference the *I-V* characteristic curve. By adjusting total probe current to correspond to $(V_f)_{\rm min}=-25.05\pm 1.5$ V when plasma potential is at $(V_p)_{\rm min}$ and to $(V_f)_{\rm max}=17.05\pm 1.5$ V, when plasma potential is at $(V_p)_{\rm max}$ the calibrated total probe current versus (V_b+V_f) is obtained. From the above calibration procedure ion saturation current was determined to be -23 ± 11.6 μA. The electron current is derived from the calibrated total probe current.

Electron current was obtained by subtracting out an esti-

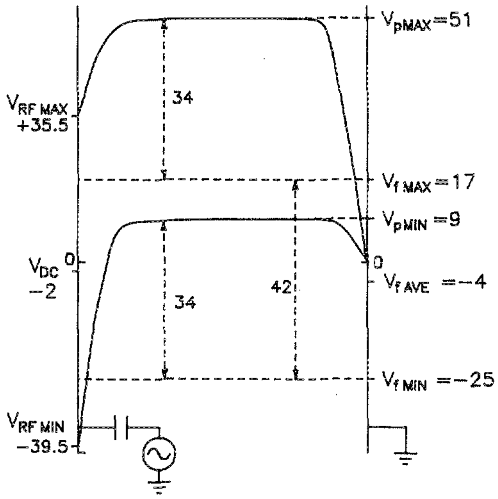

FIG. 5. Theoretical cross-sectional plasma potential distribution between powered and grounded electrode showing measured values of V_p and V_f at maximum and minimum plasma potential at device midplane. $V_p=[21\sin(\omega t)+30]V\pm 1.6$ V. $V_f=[21\sin(\omega t)-4]V\pm 1.5$ V. $V_{\rm rf}=[37.5\sin(\omega t)-2]V\pm 1.0$ V.

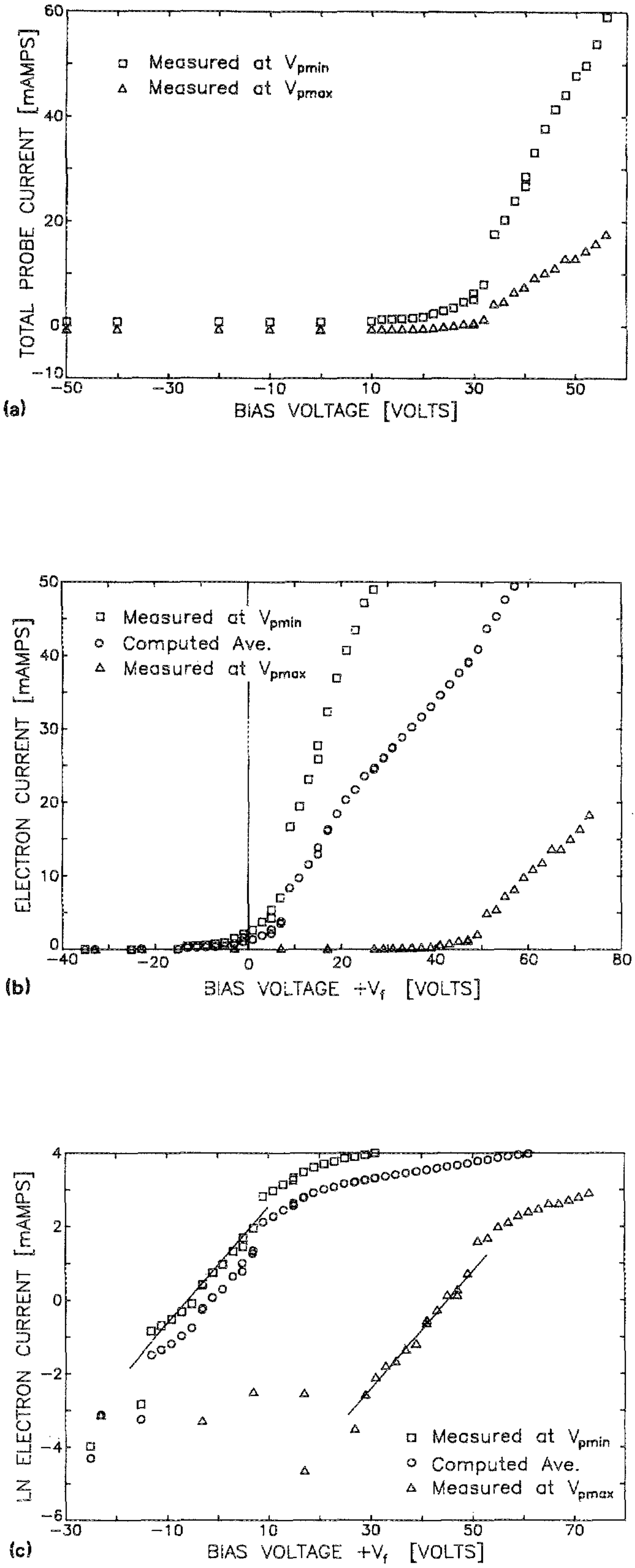

FIG. 6. (a) Unreferenced instantaneous total probe current vs V_b. Errors range from 25% for the low current values to 1% for high values of current. (b) Instantaneous and calculated average electron current vs (V_b+V_f). (c) Natural log of instantaneous and calculated average electron current vs (V_b+V_f) The slope of the line drawn through $\ln(I_e)$ at $(V_p)_{\rm min}$ and $(V_p)_{\rm max}$ in the exponential region is T_e at the V_p extrema. T_e at $(V_p)_{\rm min}=6.49\pm 0.19$ eV. T_e at $(V_p)_{\rm max}=6.85\pm 0.19$ eV. $T_{e\,\rm ave}=6.46\pm 0.24$ eV.

mate of ion current from the total probe current data. An analysis determining the ion current component and its effects on calculating I_e and $\ln(I_e)$ has been conducted.[24] A combination of the constant subtraction method and linear subtraction method was chosen for this work. The constant selected was the ion saturation value of $-23\,\mu$A. The linear approximation was chosen from $V_{I\,\mathrm{sat}}$ to V_p were $I_i = I_{\mathrm{sat}}$ at $V_{I\,\mathrm{sat}}$, and $I_i = 0.0$ at V_p. Figure 6(b) is a plot of electron current, (I_e) vs $(V_b \pm V_f)$. Figure 6(c) is the natural log of electron current, $\ln(I_e)$ vs $(V_b + V_f)$. The left-hand side of each plot is instantaneous current at $(V_p)_{\min}$ occurring at 9 ± 1.6 V and the right-hand side is instantaneous current at $(V_p)_{\max} = 51 \pm 1.6$ V.

The calculated averages of I_e and $\ln(I_e)$ between the two extremes of $(V_p)_{\min}$ and $(V_p)_{\max}$ are also shown in Fig. 6(a) and 6(b), respectively. Because each current data point, corresponding to a particular voltage for instantaneous current at $(V_p)_{\min}$ [see Fig. 6(a)], is not the same voltage for a current data point at $(V_p)_{\max}$, a linear approximation was used to acquire corresponding data points. From this expansion of data points an average current was derived. In this case the respective average plots closely approximate the shapes of the instantaneous curve for $(V_p)_{\min}$. This is because of the large spread along the V axis between the instantaneous I–V for $(V_p)_{\min}$ and $(V_p)_{\max}$. Therefore, in this case the electron temperature obtained from the average I–V trace is the same as that obtained from the instantaneous I–V trace. However, if $(V_p)_{\max} - (V_p)_{\min}$ were smaller, the average I–V trace would not provide an accurate determination of plasma parameters. The V_p for the average I–V curve is not equal to $[(V_p)_{\min} + (V_p)_{\max}]/2$. To obtain average plasma potential the instantaneous plot of I-V is required.

The electron temperatures obtained by linear regression analysis were T_e at $(V_p)_{\min} = 6.49 \pm 0.19$ eV, T_e at $(V_p)_{\max} = 6.58 \pm 0.19$ eV, and $T_{e\,\mathrm{ave}} = 6.46 \pm 0.24$ eV. Note that the electron temperature is the same at the plasma potential extrema.

The results from the Laframboise iteration method[25] and Eq. (1) were used to calculate N_e. In this case $j_i^* = 2.9$ to obtain a density of $1.48 \pm 0.83 \times 10^{10}$ electrons/cm^3. R_p/l_d and l_{mfp}/l_d were determined to be 1.2 and 2.0, respectively. This implies that these measurements occurred in the conventional Langmuir probe and near orbital motion limited regime.[24]

V. SUMMARY

Three probes were used to obtain plasma parameters for an argon plasma excited at 60-W coupled power at 13.56 MHz. Because of wide spread between $(V_p)_{\min}$ and $(V_p)_{\max}$, the average I–V characteristic closely follows instantaneous I–V at $(V_p)_{\min}$. Therefore, average T_e equals instantaneous T_e at plasma potential extrema. Plasma potential from the average I–V curve is not the average of the plasma potential extrema. $V_p = [21\sin(wt) \pm 30] \pm 1.6$ V at the chamber midplane. An independent method of measuring V_f is required to reference the I–V characteristic. $V_f = [21\sin(wt) - 4] \pm 1.5$ V. A consistency check for $V_p - V_f$ was obtained from[5]

$$V_p - V_f = (kT_e/2e)\{\ln[(1/2\pi X^2)(M_i/M_e)]\},$$

where X is a function of T_i/T_e, usually $= 0.6$, using $X = 0.575$ for $T_i/T_e = 0.004$, and $T_e = 6.5 \pm 0.3$ eV.

$$V_p - V_f = 34.0 \pm 1.6\ \mathrm{V}.$$

This falls within the measured value of 34 ± 0.5 V.

Future work will be conducted to determine variation in plasma potential throughout the device cross section, and T_e and N_e at the plasma potential null.

ACKNOWLEDGMENTS

Financial support for this research was obtained from Presidential Young Investigator Award/National Science Foundation Grant No. NSF-CBT-84-51599. We would also like to express our gratitude for the donation of the Davis and Wilder etcher by Intel corporation, and the Tegal power supply by Motorola corporation. Furthermore we would like to thank Bruce Cain, Ph.D. candidate in Nuclear Engineering at the University of Illinois, for his valuable assistance and advice during the course of this project.

[1] I. Langmuir and H. M. Mott-Smith, Gen. Electr. Rev. **27**, 449, 538, 616, 762, and 810 (1924).
[2] H. M. Mott-Smith and I. Langmuir, Phys. Rev. **28**, 727 (1926).
[3] *Plasma-Diagnostics Techniques*, edited by F. F. Chen, R. H. Huddleston, and S. L. Leonard (Academic, New York, 1964), Chap. 4.
[4] *Plasma Diagnostics*, edited by L. Schott and W. Lochte-Holtgrave (Wiley, New York, 1968), Chap. 11.
[5] J. W. Swift and M. J. R. Schwar, *Electrical Probes for Plasma Diagnostics* (Iliffe, London, 1970).
[6] R. S. Harp, Rev. Sci. Instrum. **34**, 416 (1963).
[7] F. F. Chen, Rev. Sci. Instrum. **35**, 1208 (1964).
[8] B Chapman, *Glow Discharge Processes* (Wiley, New York, 1980), Chap. 5.
[9] N. Hershkowitz, M. H. Cho, C.-H. Nam, and T. Intrator, Plasma Chem. Plasma Process. **8**(1), 35 (1988).
[10] E. O. Johnson and L. Malter, Phys. Rev. **80**, 58 (1950).
[11] J. Polman, Physica **34**, 310 (1967).
[12] F. F. Chen, "Modern Uses of Langmuir Probes," Institute of Plasma Report No. IPPJ-750, 1985.
[13] A. Boschi and F. Magistrelli, Nuovo Cimento **29**(2), 487 (1963).
[14] J. O. Swift, Brt. J. Appl. Phys. (J. Phys. D), Ser. 2 **2**, 134 (1969).
[15] N. Benjamin, Rev. Sci. Instrum. **53**, 1541 (1982).
[16] J. B. O. Caughman II, D. N. Ruzic, and D. J. Hoffman, J. Vac. Sci. Technol. 7, 1092 (1989) (these proceedings).
[17] E. Y. Wang, N. Hershkowitz, T. Intrator, and C. Forest, Rev. Sci. Instrum. **57**, 2425 (1986).
[18] W. E. Yao, T. Intrator, and N. Hershkowitz, Rev. Sci. Instrum. **56**, 519 (1969).
[19] J. R. Smith, N. Hershkowitz, and P. Coakley, Rev. Sci. Instrum. **50**, 210 (1979).
[20] S. Iizuka, P. Michelsen, J. Juul Rasmussen, R. Schrittwieser, R. Hatakeyama *et al.*, J. Phys. E **14**, 1291 (1981).
[21] J. T. Tang, C. Kim, R. Stenzel, and L. L. Higgins, Rev. Sci. Instrum. **50**, 1458 (1979).
[22] N. Hershkowitz and M. H. Cho, J. Vac. Sci. Technol. A **6**, 2054 (1988).
[23] R. J. Smith, *Circuits Devices and Systems*, 3rd ed. (Wiley, New York, 1976), Chap. 2.
[24] B. L. Cain, "Electric Probe Data Analysis for Glow Discharge Diagnostics," Master's thesis, University of Illinois, 1987.
[25] J. G. Laframboise, University of Toronto Institute of Aerospace Studies Report No. 100, 1966.
[26] F. F. Chen, Proceedings of Conference on Physics of Quiescent Plasmas, Frascati, Part II, 1967, p. 563.